Talanta 294 (2025) 128142

Contents lists available at ScienceDirect

Talanta

journal homepage: www.elsevier.com/locate/talanta

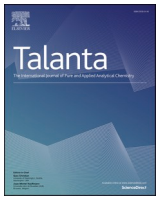

Diverse pore-sized sulfonic acid covalent organic frameworks for solid-phase extraction of fluoroquinolones in food samples

Shi-qi Ao [b], Shuang-Ping Liu [a], Yun Jiang [d], Xiu-Ping Yan [a,b,c], Hai-Long Qian [a,b,*]

[a] State Key Laboratory of Food Science and Resource, Jiangnan University, Wuxi, 214122, China
[b] Institute of Analytical Food Safety, School of Food Science and Technology, Jiangnan University, Wuxi, 214122, China
[c] Key Laboratory of Synthetic and Biological Colloids, Ministry of Education, Jiangnan University, Wuxi, 214122, China
[d] Department of Light Chemical Engineering, Jiangnan University, Wuxi, 214122, China

ARTICLE INFO

Handling Editor: Qun Fang

Keywords:
Sulfonic acid functionalized covalent organic frameworks
Pore sizes
Solid-phase extraction
Fluoroquinolones
Adsorption

ABSTRACT

Tuning the pore size of covalent organic frameworks (COFs) to achieve maximum adsorption performance is an effective way for promoting the enrichment of trace fluoroquinolones (FQs) in food, but it remains challenging. Herein, we prepare three pore-sized sulfonic acid functionalized COFs (SF-COFs), named TPS, TBS, and TSS, to investigate the effect of pore size on the adsorption efficiency of FQs. These three SF-COFs exhibit excellent adsorption capacities for FQs including enrofloxacin (ENR), norfloxacin (NOR), and ciprofloxacin (CIP). Notably, TBS achieves a maximum adsorption capacity of 627.3 mg g^{-1} for NOR, resulting from its suitable pore size (1.6 times larger than the size of FQs). Accordingly, we further develop a novel TBS based solid-phase extraction to couple with high-performance liquid chromatography for determination of FQs in various foods, which achieves rapid extraction (10 min), low detection limits (0.007–0.01 ng mL^{-1}), wide linear range (0.1–1000 ng mL^{-1}), and good recoveries (83.7%–105.2%).

1. Introduction

Quinolones have now become a major class of artificially synthesized anti-infective drugs and been widely used in clinical practice due to their broad spectrum, high efficiency, and low toxicity [1,2]. Fluoroquinolones (FQs), as the third-generation quinolones, are characterized by a fluorine atom at the 6-position and a piperazine ring at the 7-position of the quinolone naphthyridine ring [3]. FQs are well-known for their efficacy against Staphylococcus, Streptococcus pneumoniae, certain anaerobic bacteria, and Mycoplasma, especially Pseudomonas aeruginosa, thereby are widely applied as specific antibiotics in agricultural and veterinary drugs [4–8]. However, the FQs residues have emerged as a significant environmental and food safety concern due to their widespread detection in water, soil, and food products, as well as their potential ecological risks and health hazards (e.g., toxic to aquatic organisms). Additionally, these residues also accelerate the development of antibiotic resistance in bacteria, further compromising environmental and public health. Currently, many countries and regions have restricted the maximum residue levels of FQs in foods [5,9–12]. However, the trace level of FQs and severe interferences from the complex food matrix greatly prevent the precise determination of FQs in foods [13–16].

Solid adsorbent-based extraction not only enables the enrichment of trace analytes but also effectively eliminates matrix interference, making it essential for the determination of FQs [17]. However, traditional adsorbents, including activated carbon, alumina, polyacrylamide, and zeolite molecular sieves, exhibit low selectivity and adsorption efficiency for FQs, because of the size mismatching, lack of surface polarity, and insufficient chemical interactions [18–20]. Covalent organic frameworks (COFs) are a novel class of crystalline covalent bond-linked porous materials [21]. COFs exhibit periodic structures with large surface areas and adjustable pore environments, enabling their wide applications in gas storage, separation, catalysis, and sensing [21–26]. The COFs structure and their specific interactions between COFs and target molecules can be tailored through rational design of the building blocks or functional groups. Therefore, COFs with high selectivity and adsorption capacity can be designed according to the properties of target.

To date, various functional COFs have been applied as adsorbents for the extraction of FQs [27,28]. For instance, sulfonic acid groups were introduced into COFs to bring strong electrostatic interactions for FQs to couple with the inherent hydrogen bonding and π-π interactions. These

* Corresponding author. Institute of Analytical Food Safety, School of Food Science and Technology, Jiangnan University, Wuxi, 214122, China.
E-mail address: hlqian@jiangnan.edu.cn (H.-L. Qian).

https://doi.org/10.1016/j.talanta.2025.128142
Received 8 March 2025; Received in revised form 7 April 2025; Accepted 12 April 2025
Available online 18 April 2025

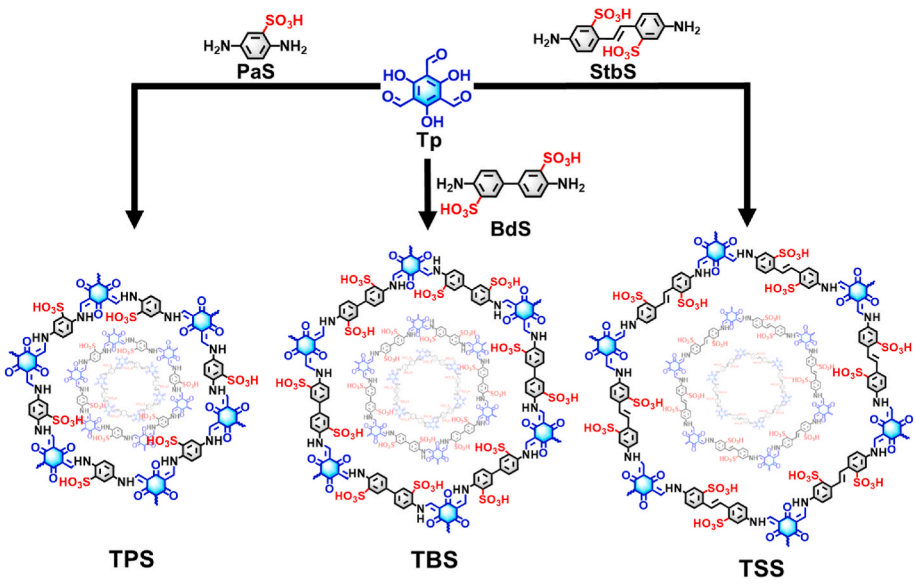

Fig. 1. Illustration for the synthesis of TPS, TBS, and TSS.

modifications enhanced the selectivity of COFs for FQs and minimized interference from complex matrices [29–32]. In addition, the pore size of COFs also significantly influences their adsorption performance. Small pores can be easily blocked by entangled target molecules, while excessively large pores weaken the adsorption binding energy between the COFs and target molecules [33–35]. This leads to a significant reduction in adsorption efficiency. Therefore, determining the optimal pore size of COFs to maximize adsorption performance for FQs remains a significant challenge, that has not yet been investigated.

Herein, we rationally prepared three pore-sized sulfonic acid functionalized COFs (SF-COFs), named TPS, TBS, and TSS, to investigate the effect of pore size on the adsorption efficiency of FQs. The TPS, TBS, and TSS were synthesized using the same monomer 1,3,5-triformylphloroglucinol (Tp) to react with 2,5-diamino benzene sulfonic (PaS), 4,4′-diamino-3,3′-biphenyldisulfonic acid (BdS), and 4,4′-diaminostilbene-2,2′-disulfonic acid (StbS), respectively. Then, the adsorption performance of FQs on these three SF-COFs was further studied. Finally, an SF-COF-based solid phase extraction coupled with HPLC-FLD was developed for the determination of FQs in various real food samples. This study provides a promising method for selecting COFs with suitable pore sizes for selective extraction of FQs in food samples.

2. Materials and methods

2.1. Reagents

All reagents and solvents were used without further purification. Tp, PaS, BdS and StbS were purchased from the Aladdin Bio-Chem Technology Co., Ltd. (Shanghai, China). Enrofloxacin (ENR), norfloxacin (NOR), ciprofloxacin (CIP), cefalexin (CL), sulfamethoxazole (SMZ), and oxolinic acid (OA) were bought from ANPEL laboratory technologies Co., Ltd. (Shanghai, China). Acetone, ethanol, tetrahydrofuran (THF), acetic acid (HAc, 99 %), methanol (MeOH), acetonitrile (ACN), mesitylene, and 1,4-dioxane were obtained from Sinopharm Chemical Reagent Co., Ltd. (Shanghai, China). 0.22 μm membrane was bought from Agilent Technologies Co., Ltd. (Shanghai, China).

2.2. Synthesis of SF-COFs

Three SF-COFs with different pore sizes were synthesized using the reported methods with slight modifications [29,35,36]. Briefly, mesitylene (1.2 mL), 1,4-dioxane (0.3 mL), Tp (31.5 mg), PaS (42.3 mg), and 6.0 M acetic acid (0.3 mL) were mixed and sonicated for 15 min, then flash-frozen at 77 K, and finally heated at 120 °C for 3 days. The produced red solid was collected by filtration, and washed with acetone, THF, and then MeOH, respectively. The final TPS was obtained after drying in a vacuum at 60 °C overnight (yield: 81.6%). The preparation of TBS and TSS followed a similar process to that of TPS. For TBS, BdS (77.4 mg) was used instead of PaS, yielding 84.1%. For TSS, PaS was replaced with StbS (83.3 mg), and the amounts of mesitylene and 1, 4-dioxane were increased to 1.5 mL and 0.5 mL, respectively. The obtained yield of TSS was 69.2%.

2.3. Adsorption experiments

Typically, 1 mg of SF-COF was dispersed in 4 mL of FQs solution (pH 6.0). The mixture was shaken for a certain time till adsorption equilibrium and then centrifuged at 10000 rpm. The collected supernatant was filtered by a 0.22 μm filter membrane. The FQs in the collected solution were detected with UV–vis absorption spectroscopy. More details were described in Supplementary Information.

2.4. Procedures for solid-phase extraction

10 mg of TBS was mixed with 20 mL of FQs standard or real sample solution under shaking for 10 min. Then TBS was collected by centrifugation and subsequently rinsed using 2 mL of 1 M HAc and ACN (3:7, v/v). The collected eluate was filtered with a 0.22 μm membrane, dried with nitrogen, and dissolved in 0.1 mL of MeOH for further analysis. The FQs were detected using HPLC-FLD equipped with a C18 chromatographic column. The separation condition was as follows: Mobile phase, water-ACN (80:20, v/v, containing 0.1 % trifluoroacetic acid); flow rate, 0.7 mL min^{-1}; excitation at 280 nm and emission at 450 nm for the fluorescence detector.

2.5. Food sample analysis

Food samples including milk, honey, egg, shrimp, pork, and fish were purchased from local supermarkets. 5 g of liquid samples (milk, honey, and egg) were accurately weighed and then mixed with 20 mL of ACN under ultrasonication for 30 min. For solid samples (shrimp, pork, and fish), 5 g of samples were accurately weighed and chopped, mixed with 20 mL of ACN vortexing for 1 min, and further ultrasonicated for 30 min. Both liquid and solid samples were then centrifuged at 10000 rpm for 5

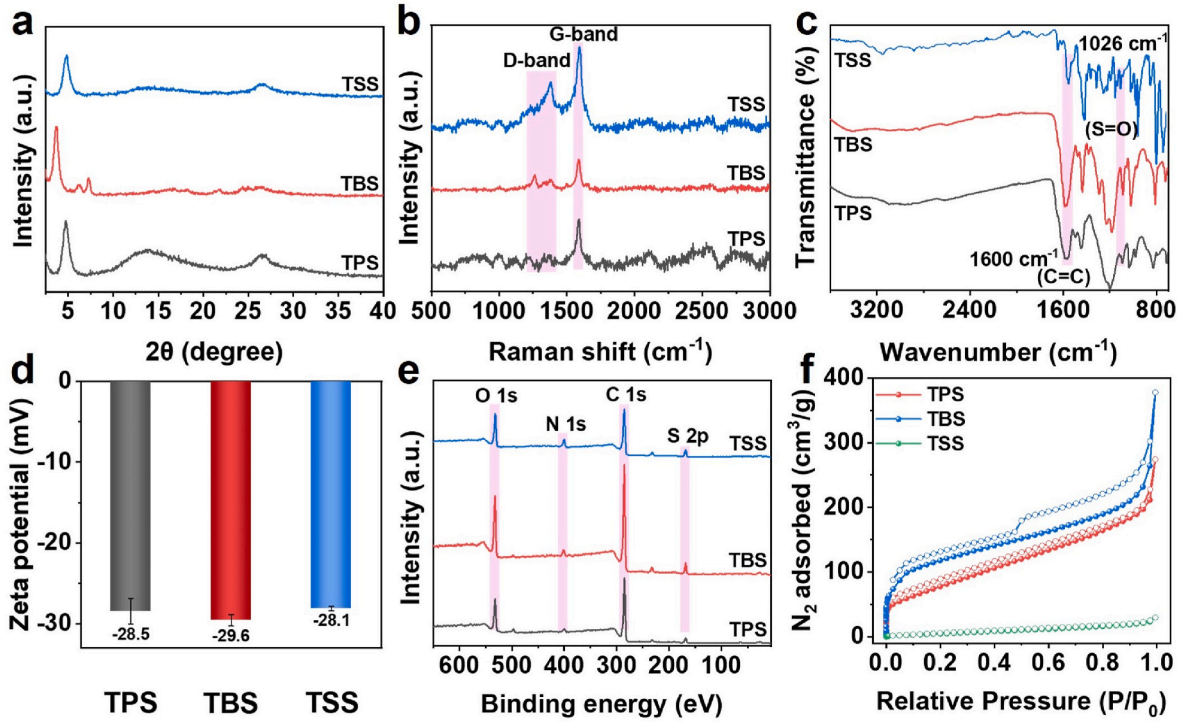

Fig. 2. (a) PXRD patterns, (b) Raman spectra, (c) FTIR spectra, (d) Zeta potential, (e) XPS spectra, and (f) Nitrogen adsorption-desorption isotherms of SF-COFs.

min to collect the supernatant. After being filtered with a 0.22 μm filter membrane, the supernatant was dried with nitrogen. The collected residues were dissolved in 0.1 mL MeOH and made up to 20 mL with water (pH 6.0) for subsequent SPE and analysis.

3. Results and discussion

3.1. Preparation and characterization of SF-COFs

Three sulfonic acid-functionalized diamine monomers with varying molecular lengths (PaS, BdS, and StbS) were condensed with the aldehyde monomer of Tp to synthesize diverse pore-sized SF-COFs, named TPS, TBS, and TSS, respectively (Fig. 1). The similar linear configurations but differing lengths of PaS, BdS, and StbS resulted in the same topological structures for the prepared TPS, TBS, and TSS, but different pore sizes. In addition, the introduced sulfonic acid groups can serve as specific binding sites, enabling efficient adsorption of FQs through electrostatic interactions and hydrogen bonding.

The appearance of intense peaks in powder X-ray diffraction (PXRD) patterns of TPS, TBS, and TSS confirmed their ordered two-dimensional

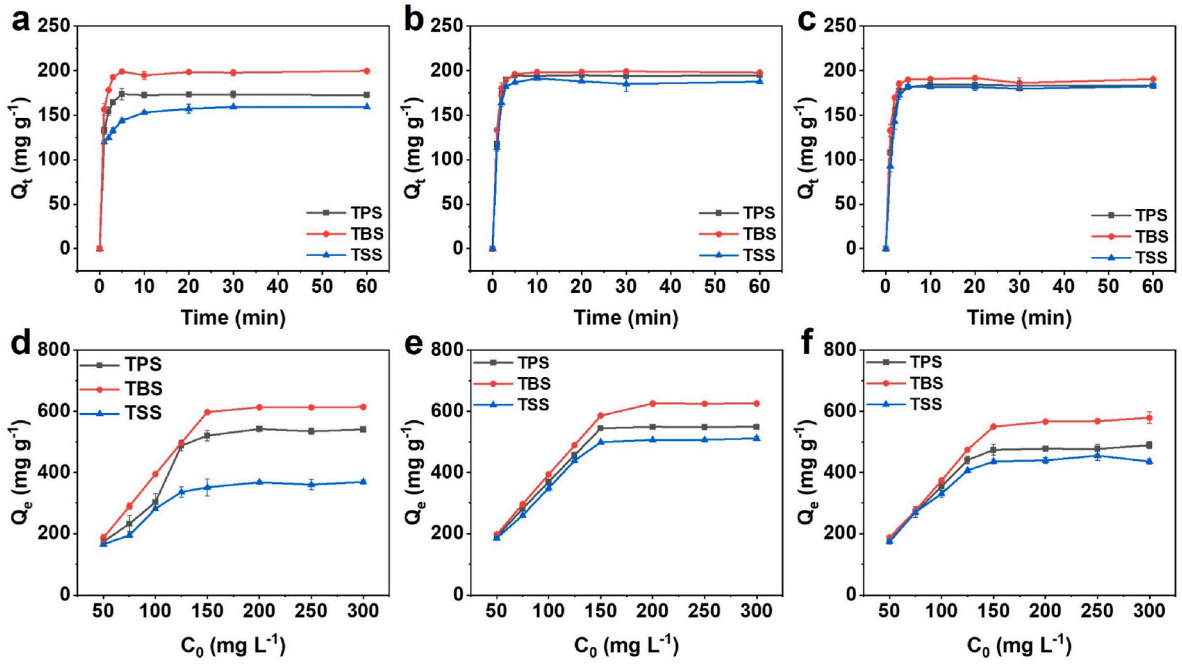

Fig. 3. Adsorption kinetics curves of SF-COFs for (a) ENR, (b) NOR, and (c) CIP. Adsorption isotherms of SF-COFs for (d) ENR, (e) NOR, and (f) CIP.

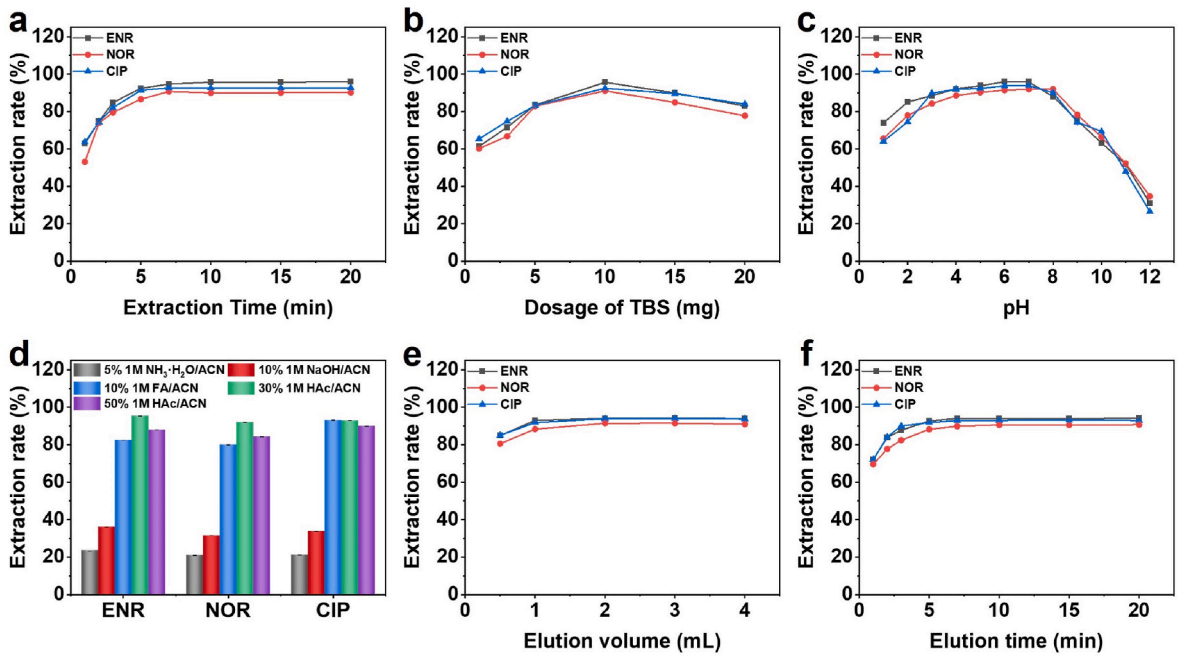

Fig. 4. Optimization of extraction and desorption parameters: (a) Extraction time. (b) Dosage of adsorbent. (c) pH of sample solution. (d) Elute solvent. (e) Elution volume. (f) Elution time.

crystalline structures. The relatively low rigidity of StbS resulted in reduced π-π stacking interaction and low crystallinity of TSS (Fig. 2a). In addition, all three COFs showed the presence of the D and G band in their Raman spectra (Fig. 2b). The intensity ratios of the D-band to G-band (I_D/I_G) for TPS, TBS, and TSS were 0.02, 0.31, and 0.52, respectively. The smallest I_D/I_G indicates superior lattice symmetry and the fewest defects of TPS.

The observation of characteristic peaks in Fourier transform infrared (FTIR) spectra of TPS, TBS, and TSS at 1597, 1598, and 1600 cm^{-1} (assigned to the C═C), along with the absence of peaks for C═N, indicates the typical transformation of the enol structure to the keto structure during the formation of COFs. The appearance of the stretching band at 1026 cm^{-1}, 1023 cm^{-1}, and 1030 cm^{-1} for TPS, TBS, and TSS served as evidence for the presence of sulfonic acid groups in the prepared COFs (Fig. 2c and S1). Zeta potentials of all three SF-COFs were significantly negative (−28.5, −29.6, and −28.1 mV), resulting from the existence of the sulfonic acid groups (Fig. 2d). All the TPS, TBS, and TSS gave obvious S 2p peaks in their X-ray photoelectron spectroscopy (XPS) patterns, further confirming the sulfonate groups in the three proposed SF-COFs (Fig. 2e).

N_2 adsorption-desorption isotherms of the SF-COFs can be described as type IV behavior, indicating the presence of mesoporous structures in the SF-COFs (Fig. 2f). The BET surface areas of TPS, TBS, and TSS were calculated to be 275 $m^2\ g^{-1}$, 373 $m^2\ g^{-1}$, and 26.49 $m^2\ g^{-1}$, respectively (Fig. S2). The low surface area of TSS was potentially due to its relatively poor crystallinity [37,38]. The main pore size distributions of TPS, TBS, and TSS using the nonlocal density functional theory model centered at 1.85 nm, 2.20 nm, and 2.58 nm, respectively (Fig. S3). Scanning electron microscopy (SEM) revealed both TPS and TBS possessed layer-like morphologies, while TSS exhibited a spherical morphology (Fig. S12a-S12c).

3.2. Adsorption performance and pore size-related adsorption mechanism

The adsorption performance of SF-COFs was evaluated using three widely prescribed FQs: ENR, NOR, and CIP. All three SF-COFs exhibited pH-dependent adsorption behavior, with capacities initially increasing and reaching maximum values at pH 6.0. Further increase in pH led to a decline in adsorption capacity (Fig. S4). Accordingly, the adsorption kinetics of three COFs for ENR, NOR, and CIP were conducted at pH 6.0. The adsorption capacity (Q_t) of ENR, NOR, and CIP on the three SF-COFs increased sharply in the first 3 min and reached equilibrium within 5 min (Fig. 3a–c). The adsorption kinetics were poorly described by the pseudo-first-order model ($R^2 < 0.9$). In contrast, the pseudo-second-order kinetic model showed excellent agreement with the experimental data, suggesting the predominant chemisorption between the three SF-COFs and FQs (Fig. S5). TBS possessed larger rate constants (0.024, 0.038, and 0.035 g $mg^{-1}\ min^{-1}$) for three FQs, than those of TPS (0.023, 0.032, and 0.029 g $mg^{-1}\ min^{-1}$) and TSS (0.011, 0.028, and 0.017 g $mg^{-1}\ min^{-1}$), suggesting superior adsorption kinetics for FQs. (Table S1–S3).

The adsorption isotherms of ENR, NOR, and CIP on the three SF-COFs fitted well with the Langmuir isotherm adsorption model rather than the Freundlich isotherm adsorption model (Fig. 3d–f and Fig. S6), indicating their uniform monolayer adsorption. Additionally, the theoretical maximum adsorption capacities (Q_{max}) of TBS obtained from the Langmuir model fitting for ENR, NOR, and CIP are 616.9 mg g^{-1}, 627.3 mg g^{-1}, and 575.0 mg g^{-1}, respectively, which were superior to those of the other two SF-COFs (Table S4–S6). For instance, the Q_{max} of TBS for ENR is 1.6 times that of TSS (377.0 mg g^{-1}) and 1.1 times that of TPS (547.0 mg g^{-1}) (Table S7).

Although the pore sizes of the three SF-COFs (1.85–2.58 nm) were larger than the FQs (1.34–1.44 nm) (Fig. S7), TBS gave the best adsorption performance for ENR, NOR, and CIP. The pore size of TPS (1.85 nm) was similar to molecular sizes of the three FQs, which can cause a pronounced steric hindrance effect that limited the adsorption. The larger pore of TBS (2.20 nm), about 1.6 times larger than the three FQs, eliminated the diffusion obstruction associated with small-pore molecules, leading to the enhanced adsorption. However, further pore size increase would weaken the binding affinity of SF-COFs. This dominantly explained why TSS (2.58 nm) with the largest pores exhibited the lowest adsorption capacity for the three FQs. Accordingly, SF-COFs with pores about 1.6 times larger than the molecular size of FQs are more conducive to adsorption.

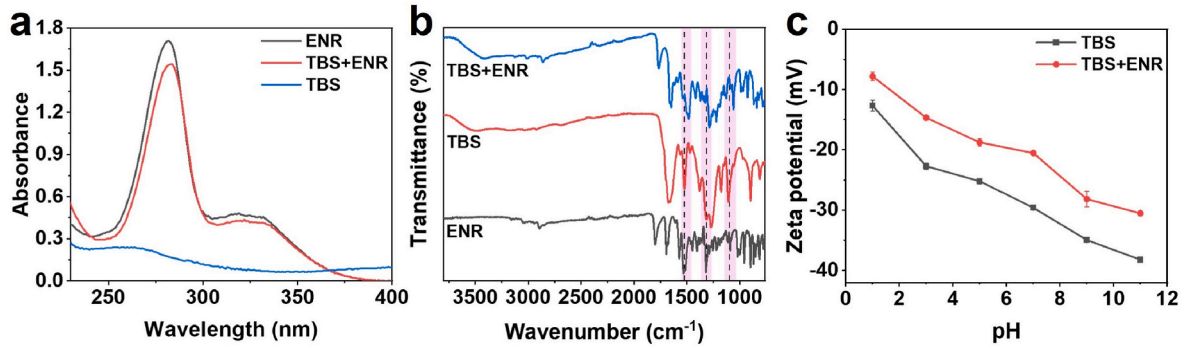

Fig. 5. (a) UV–vis spectroscopy and (b) FT-IR spectroscopy of ENR, TBS before and after the adsorption of ENR. (c) Zeta potentials at different pH before and after ENR adsorption of TBS.

3.3. TBS-based solid-phase extraction

The excellent adsorption performance of TBS for FQs encouraged us to apply it as an adsorbent for the extraction of FQs. Extraction rate of FQs stabilized at 10 min, indicating the complete extraction (Fig. 4a). The extraction rate initially increased with the amount of TBS from 0 to 10 mg, but declined at higher amounts due to restricted FQs diffusion caused by excessive adsorbent. Consequently, 10 mg of TBS was identified as the optimal amount for subsequent extraction (Fig. 4b). The extraction rate reached maximum at pH 6.0, driven by enhanced electrostatic interactions between sulfonic acid and amino groups (Fig. 4c). Similarly, the optimized elution using the extraction rate as the evaluation metric was achieved with 2 mL of 1 M HAc and ACN (3:7, v/v) as eluent under stirring for 7 min (Fig. 4d–f).

In the presence of negatively charged OA, positively charged SMZ, and zwitterionic CL, TBS maintained great extraction efficiency for ENR, NOR, and CIP, proving its good selectivity (Fig. S8 and S9). Furthermore, ENR was selected as a model target to investigate the interactions between FQs and TBS. A red shift of the UV–visible absorption peak of TBS from 271 to 273 nm, as well as a distinct shift in the aromatic ring stretching characteristic FTIR peak of TBS from 1517 cm^{-1} to 1513 cm^{-1} after the adsorption of ENR served as the direct evidence of the π-π stacking interaction between the intrinsic benzene rings of TBS and ENR (Fig. 5a–b) [32,39]. Additionally, the characteristic S═O asymmetric bands at 1266 cm^{-1} and 1020 cm^{-1} in FTIR spectra of TBS shifted to 1260 cm^{-1} and 1017 cm^{-1}, respectively, demonstrating the formation of hydrogen bonds between TBS and ENR (Fig. 5b) [29,30]. The embedded sulfonic acid groups conferred negative charges upon TBS within a wide pH range of 1.0–11.0. After the adsorption of ENR, the surface zeta potential of TBS evidently increased, resulting from the electrostatic interaction between the positively charged amino group of ENR and the negatively charged sulfonic acid groups of TBS (Fig. 5c) [18,31].

3.4. Analytical performance

The TBS-based solid-phase extraction was coupled with high-performance liquid chromatography-fluorescence detection (TBS-SPE-HPLC-FLD) for the determination of FQs. The developed TBS-SPE-HPLC-FLD method exhibited broad linear ranges (0.1–1000 ng mL^{-1}) for determining the three FQs ($R^2 > 0.9995$). The limits of detection (LODs, S/N = 3) and limits of quantitation (LOQs, S/N = 10) of TBS-SPE-HPLC-FLD for the three FQs were 0.007–0.01 ng mL^{-1} and 0.022–0.03 ng mL^{-1}, respectively. The intraday and interday RSDs for the detection of FQs (100 ng mL^{-1}) were 1.09%–2.17% and 1.39%–2.25%, respectively

Table 1
Analytical results for FQs determination in food samples (mean ± *s*, *n* = 5).

Samples	Spiked (μg kg^{-1})	ENR		NOR		CIP	
		Determined (μg kg^{-1})	Recovery (%)	Determined (μg kg^{-1})	Recovery (%)	Determined (μg kg^{-1})	Recovery (%)
Milk	0	1.2 ± 0.2	–	0.5 ± 0.1	–	<LOQ	–
	10	10.5 ± 0.3	93.4 ± 3.2	9.9 ± 0.1	94.8 ± 1.4	9.5 ± 0.2	95.2 ± 2.1
	50	50.6 ± 0.5	98.9 ± 0.9	48.8 ± 0.6	96.7 ± 1.3	48.4 ± 0.9	96.9 ± 1.9
	250	248.3 ± 1.8	98.8 ± 0.8	244.9 ± 1.2	97.8 ± 0.5	242.3 ± 1.0	97.0 ± 0.4
Honey	0	ND[a]	–	ND[a]	–	ND[a]	–
	10	9.7 ± 0.5	97.3 ± 4.8	8.9 ± 0.7	89.2 ± 7.4	10.1 ± 0.1	100.7 ± 1.1
	50	45.9 ± 0.9	91.9 ± 1.8	47.8 ± 1.6	95.7 ± 3.3	50.8 ± 0.4	101.6 ± 0.7
	250	240.3 ± 1.8	96.1 ± 0.7	232.8 ± 1.9	93.1 ± 0.8	245.3 ± 1.0	98.1 ± 0.4
Fish	0	1.1 ± 0.1	–	0.3 ± 0.1	–	ND[a]	–
	10	10.7 ± 0.6	96.4 ± 5.7	10.1 ± 0.1	98.1 ± 0.9	9.1 ± 0.4	90.8 ± 3.9
	50	50.8 ± 0.9	99.5 ± 1.7	49.3 ± 0.7	98.2 ± 1.3	47.6 ± 0.8	95.3 ± 1.6
	250	251.0 ± 1.5	100.0 ± 0.6	245.2 ± 0.8	98.0 ± 0.3	233.6 ± 2.3	93.4 ± 0.9
Shrimp	0	<LOQ	–	ND[a]	–	ND[a]	–
	10	9.9 ± 0.3	99.3 ± 3.1	9.6 ± 0.8	96.3 ± 7.6	10.2 ± 0.4	102.1 ± 4.3
	50	48.9 ± 1.0	97.9 ± 2.1	47.3 ± 2.3	94.6 ± 4.7	52.0 ± 1.5	104.1 ± 3.1
	250	242.5 ± 2.4	97.0 ± 0.9	246.4 ± 2.0	98.6 ± 0.8	253.4 ± 2.7	101.4 ± 1.1
Pork	0	3.6 ± 0.4	–	<LOQ	–	ND[a]	–
	10	14.1 ± 0.9	105.2 ± 8.8	8.8 ± 0.1	88.7 ± 1.2	9.1 ± 0.4	91.3 ± 4.0
	50	55.1 ± 2.2	103.0 ± 4.3	45.4 ± 0.3	90.8 ± 0.5	44.8 ± 0.2	89.7 ± 0.4
	250	248.8 ± 2.8	98.1 ± 1.1	229.9 ± 2.5	92.0 ± 1.0	228.5 ± 3.7	91.4 ± 1.5
Egg	0	ND[a]	–	ND[a]	–	ND[a]	–
	10	9.2 ± 0.7	92.3 ± 7.1	9.0 ± 0.8	89.6 ± 7.9	8.4 ± 0.1	83.7 ± 0.9
	50	46.5 ± 0.8	93.1 ± 1.5	44.6 ± 1.5	89.3 ± 2.9	42.9 ± 0.3	85.7 ± 0.6
	250	238.2 ± 1.3	95.3 ± 0.5	220.7 ± 2.9	88.3 ± 1.2	230.6 ± 0.9	92.3 ± 0.4

[a] Not detected.

(Table S8). This proposed method demonstrated superior performance compared to previously reported methods for determining FQs (Table S9). Furthermore, the representative TBS possessed good recyclability for the slight reduction in extraction capacity (Fig. S10) owing to no apparent change in crystalline structure and morphology (Fig. S11 and S12).

3.5. Food sample analysis

The practical ability of the TBS-SPE-HPLC-FLD method was further assessed by detection of FQs in several food samples including milk, honey, fish, shrimp, pork, and egg (Table 1). The matrix effect of all six real samples ranged from 0.9 to 1.0 after the extraction of TBS, indicating the great matrix interference removal capability of TBS. Moreover, the lower matrix effect also revealed that the standard calibration curve using pure water can serve as a working curve during the analysis of the six real food samples (Fig. S13). CIP was not detected in all the samples, but some samples tested positive for both ENR and NOR. 1.2 μg kg^{-1} of ENR and 0.5 μg kg^{-1} of NOR were detected in milk. 1.1 μg kg^{-1} of ENR and 0.3 μg kg^{-1} of NOR were detected in fish. And 3.6 μg kg^{-1} of ENR was detected in pork. Moreover, the levels of FQs (10, 50, and 250 μg kg^{-1}) were spiked into the above food samples and then analyzed with the developed TBS-SPE-HPLC-FLD method. The obtained recoveries ranged from 83.7% to 105.2%, indicating the great precision of the developed method for the determination of FQs in actual food samples.

4. Conclusion

In summary, three sulfonic acid functionalized covalent organic frameworks (TPS, TBS, and TSS) with different pore sizes were synthesized to investigate the adsorption performance of FQs. TBS was proved to be superior for adsorption of three typical FQs including ENR, NOR, and CIP, resulting from its optimal pore size (1.6 times larger than the size of analytes) that minimizes diffusion resistance. Furthermore, the TBS was selected as an adsorbent to develop a TBS-SPE-HPLC-FLD method for detecting trace FQs in various food samples, which featured a wide linear range, low LODs and LOQs, and good reproducibility. This study can direct the pore design of COFs for efficient extraction of contaminants in complex samples.

CRediT authorship contribution statement

Shi-qi Ao: Writing – original draft, Visualization, Methodology, Investigation, Data curation. **Shuang-Ping Liu:** Resources. **Yun Jiang:** Resources. **Xiu-Ping Yan:** Resources. **Hai-Long Qian:** Writing – review & editing, Supervision, Methodology, Conceptualization.

Declaration of competing interest

The authors declare that they have no known competing financial interests or personal relationships that could have appeared to influence the work reported in this paper.

Acknowledgments

This work was supported by the National Natural Science Foundation of China (22422406, 22376082, and 42421005), and the “Fundamental Research Funds for the Central Universities”.

Appendix A. Supplementary data

Supplementary data to this article can be found online at https://doi.org/10.1016/j.talanta.2025.128142.

Data availability

Data will be made available on request.

References

[1] T.D.M. Pham, Z.M. Ziora, M.A.T. Blaskovich, Quinolone antibiotics, Medchemcomm 10 (2019) 1719–1739.
[2] Y. Wang, X. Hui, H. Wang, H. Chen, Transcriptome deciphered the mechanisms of iron facilitating enzyme-mediated ciprofloxacin biodegradation and regulating antibiotic resistance gene dissemination through inducing gene expression, Chem. Eng. J. 488 (2024).
[3] C. Xiao, Y. Han, Y. Liu, J. Zhang, C. Hu, Relationship between fluoroquinolone structure and neurotoxicity revealed by zebrafish Neurobehavior, Chem. Res. Toxicol. 31 (2018) 238–250.
[4] Y. Zhou, J. Hu, Y. Gao, Y. Song, S.-Y. Pang, J. Jiang, Unrecognized role of humic acid as a reductant in accelerating fluoroquinolones oxidation by aqueous permanganate, Chin. Chem. Lett. 33 (1) (2022) 447–451.
[5] H. Liang, J. Zhang, J. Hu, X. Li, B. Li, Fluoroquinolone residues in the environment rapidly induce heritable fluoroquinolone resistance in Escherichia coli, Environ. Sci. Technol. 57 (2023) 4784–4795.
[6] X. Zheng, Q. Cao, Q. Cao, F. Mao, X. Li, J. Zhu, L. Lan, J. Li, Discovery of synergistic activity of fluoroquinolones in combination with antimicrobial peptides against clinical polymyxin-resistant Pseudomonas aeruginosa DK2, Chin. Chem. Lett. 31 (2) (2020) 413–417.
[7] E.L. Sweeney, K. Lowry, C. Bletchly, G.R. Nimmo, D.M. Whiley, Mycoplasma genitalium infections can comprise a mixture of both fluoroquinolone-susceptible and fluoroquinolone-resistant strains, J. Antimicrob. Chemother. 76 (2021) 887–892.
[8] E.M. Abd El-Monaem, A.S. Eltaweil, H.M. Elshishini, M. Hosny, M.M. Abou Alsoaud, N.F. Attia, G.M. El-Subruiti, A.M. Omer, Sustainable adsorptive removal of antibiotic residues by chitosan composites: an insight into current developments and future recommendations, Arab. J. Chem. 15 (2022) 103743.
[9] E. Hain, H. Adejumo, B. Anger, J. Orenstein, L. Blaney, Advances in antimicrobial activity analysis of fluoroquinolone, macrolide, sulfonamide, and tetracycline antibiotics for environmental applications through improved bacteria selection, J. Hazard Mater. 415 (2021) 125686.
[10] K.P. Mangalgiri, T. Ibitoye, L. Blaney, Molar absorption coefficients and acid dissociation constants for fluoroquinolone, sulfonamide, and tetracycline antibiotics of environmental concern, Sci. Total Environ. 835 (2022) 155508.
[11] M. Oliveira, M. Nunes, M.T. Barreto Crespo, A.F. Silva, The environmental contribution to the dissemination of carbapenem and (fluoro)quinolone resistance genes by discharged and reused wastewater effluents: the role of cellular and extracellular DNA, Water Res. 182 (2020) 116011.
[12] E.A. Serna-Galvis, S.D. Jojoa-Sierra, K.E. Berrio-Perlaza, F. Ferraro, R.A. Torres-Palma, Structure-reactivity relationship in the degradation of three representative fluoroquinolone antibiotics in water by electrogenerated active chlorine, Chem. Eng. J. 315 (2017) 552–561.
[13] S. Bhatt, S. Chatterjee, Fluoroquinolone antibiotics: occurrence, mode of action, resistance, environmental detection, and remediation - a comprehensive review, Environ. Pollut. 315 (2022) 120440.
[14] M.A.A. Masud, W.S. Shin, A. Septian, H. Samaraweera, I.J. Khan, M.M. Mohamed, M.M. Billah, E.A. Lopez-Maldonado, M.M. Rahman, A. Islam, S. Rahman, Exploring the environmental pathways and challenges of fluoroquinolone antibiotics: a state-of-the-art review, Sci. Total Environ. 926 (2024) 171944.
[15] A. Rusu, A.C. Munteanu, E.M. Arbanasi, V. Uivarosi, Overview of side-effects of antibacterial fluoroquinolones: new drugs versus old drugs, a step forward in the safety profile? Pharmaceutics 15 (2023).
[16] Y. Xie, Q. Li, L. Qin, X. Zhou, Y. Fan, Multi-templates surface molecularly imprinted polymer for simultaneous and rapid determination of sulfonamides and quinolones in water: effect of carbon-carbon double bond, Environ. Sci. Pollut. Control Ser. 28 (2021) 54950–54959.
[17] A.C. Ozelcaglayan, W.J. Parker, A.L.-T. Pham, The analysis of per- and polyfluoroalkyl substances in wastewater sludges and biosolids: which adsorbents should be used for the cleanup of extracts? Environ. Sci. Water Res. Technol. 9 (3) (2023) 794–805.
[18] X. Weng, W. Cai, G. Owens, Z. Chen, Magnetic iron nanoparticles calcined from biosynthesis for fluoroquinolone antibiotic removal from wastewater, J. Clean. Prod. 319 (2021).
[19] Q. Zhao, S. Zhang, X. Zhang, L. Lei, W. Ma, C. Ma, L. Song, J. Chen, B. Pan, B. Xing, Cation–Pi interaction: a key force for sorption of fluoroquinolone antibiotics on pyrogenic carbonaceous materials, Environ. Sci. Technol. 51 (23) (2017) 13659–13667.
[20] K. Wan, L. Huang, J. Yan, B. Ma, X. Huang, Z. Luo, H. Zhang, T. Xiao, Removal of fluoride from industrial wastewater by using different adsorbents: a review, Sci. Total Environ. (2021) 773.
[21] X.-Q. Ran, S.-T. Xu, H.-L. Qian, X.-P. Yan, Irreversible fluorine covalent organic framework based probe nanoelectrospray ionization mass spectrometry for direct and rapid determination of perfluoroalkyl carboxylic acids, J. Hazard Mater. 455 (2023).
[22] R.E. Mow, G.A. Russell-Parks, G.E.B. Redwine, B.E. Petel, T. Gennett, W. A. Braunecker, Polymer-coated covalent organic frameworks as porous liquids for gas storage, Chem. Mater. 36 (2024) 1579–1590.

[23] W.-K. Qin, C.-H. Tung, L.-Z. Wu, Covalent organic framework and hydrogen-bonded organic framework for solar-driven photocatalysis, J. Mater. Chem. A 11 (2023) 12521–12538.
[24] Y. Wang, H. Wang, Y. Liu, M. Peng, H. Fan, H. Meng, Nitrogen-containing linkage-bonds in covalent organic frameworks: synthesis and applications, Chin. Chem. Lett. (2024), https://doi.org/10.1016/j.cclet.2024.110189.
[25] Q.-Y. Mao, X.-Q. Ran, S.-T. Xu, P. Gu, Y. Jiang, X.-P. Yan, H.-L. Qian, Unlocking enhanced detection of perfluoroalkanesulfonic acids via fluorinated nonpolar 3D covalent organic frameworks-based ambient probe nanoelectrospray ionization mass spectrometry, Anal. Chem. 97 (11) (2025) 6312–6319.
[26] Y. Wang, X.-Q. Ran, C. Yang, H.-L. Qian, X.-P. Yan, Size-dependent deformation and competition H-Bond site-induced individual fluorescence response of a single-crystal three-dimensional covalent organic framework, Anal. Chem. 96 (14) (2024) 5608–5614.
[27] A. Wen, G. Li, D. Wu, Y. Yu, Y. Yang, N. Hu, H. Wang, J. Chen, Y. Wu, Sulphonate functionalized covalent organic framework-based magnetic sorbent for effective solid phase extraction and determination of fluoroquinolones, J. Chromatogr. A 1612 (2020) 460651.
[28] M. Wang, M. Gao, K. Zhang, L. Wang, W. Wang, Q. Fu, Z. Xia, D. Gao, Magnetic covalent organic frameworks with core-shell structure as sorbents for solid phase extraction of fluoroquinolones, and their quantitation by HPLC, Microchim. Acta 186 (12) (2019).
[29] W. Jiang, W.R. Cui, R.P. Liang, J.D. Qiu, Difunctional covalent organic framework hybrid material for synergistic adsorption and selective removal of fluoroquinolone antibiotics, J. Hazard Mater. 413 (2021) 125302.
[30] X. Guan, H. Li, Y. Ma, M. Xue, Q. Fang, Y. Yan, V. Valtchev, S. Qiu, Chemically stable polyarylether-based covalent organic frameworks, Nat. Chem. 11 (2019) 587–594.
[31] X. Guo, C. Kang, H. Huang, Y. Chang, C. Zhong, Exploration of functional MOFs for efficient removal of fluoroquinolone antibiotics from water, Microporous Mesoporous Mater. 286 (2019) 84–91.
[32] W. Li, N. Chen, Y. Zhu, D. Shou, M. Zhi, X. Zeng, A nanocomposite consisting of an amorphous seed and a molecularly imprinted covalent organic framework shell for extraction and HPLC determination of nonsteroidal anti-inflammatory drugs, Microchim. Acta 186 (2) (2019).
[33] Y. Zhu, T. Qiu, T. Liu, C. Li, Y. Huai, W. Ge, Simulation of gas diffusion–adsorption coupling in adsorbents for optimizing pore structures, Ind. Eng. Chem. Res. 63 (40) (2024) 17402–17412.
[34] W. Wang, Y. Jia, S. Zhou, S. Deng, Removal of typical PFAS from water by covalent organic frameworks with different pore sizes, J. Hazard Mater. 460 (2023) 132522.
[35] Y. Guo, X. Zou, W. Li, Y. Hu, Z. Jin, Z. Sun, S. Gong, S. Guo, F. Yan, High-density sulfonic acid-grafted covalent organic frameworks with efficient anhydrous proton conduction, J. Mater. Chem. A 10 (2022) 6499–6507.
[36] R. Li, X. Tang, J. Wu, K. Zhang, Q. Zhang, J. Wang, J. Zheng, S. Zheng, J. Fan, W. Zhang, X. Li, S. Cai, A sulfonate-functionalized covalent organic framework for record-high adsorption and effective separation of organic dyes, Chem. Eng. J. 464 (2023).
[37] S. Chandra, T. Kundu, K. Dey, M. Addicoat, T. Heine, R. Banerjee, Interplaying intrinsic and extrinsic proton conductivities in covalent organic frameworks, Chem. Mater. 28 (2016) 1489–1494.
[38] S. Chandra, T. Kundu, S. Kandambeth, R. Babarao, Y. Marathe, S.M. Kunjir, R. Banerjee, Phosphoric acid loaded azo (-N horizontal lineN-) based covalent organic framework for proton conduction, J. Am. Chem. Soc. 136 (2014) 6570–6573.
[39] Y. Li, C.-X. Yang, H.-L. Qian, X. Zhao, X.-P. Yan, Carboxyl-functionalized covalent organic frameworks for the adsorption and removal of triphenylmethane dyes, ACS Appl. Nano Mater. 2 (2019) 7290–7298.